Mechanisms of Ageing and Development 232 (2026) 112217

Contents lists available at ScienceDirect

Mechanisms of Ageing and Development

journal homepage: www.elsevier.com/locate/mechagedev

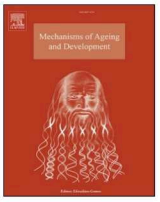

HTZ-1/H2A.Z expression sustains transcriptional programs that regulate *Caenorhabditis elegans* lifespan

Beijia Xie [a], Enzo Scifo [a], Ioanna-Maria Menegatou [a], Rossella Erminia Ciliberti [a], Mrityunjoy Mondal [a], Yiru Wang [a], Antonia Piazzesi [a], Jialu Hu [a,b], Elena De Domenico [a,c], Stefan Paulusch [a,c], Diego De Stefani [d], Matthias Schmid [a,e], Dagmar Wachten [f], Marc D. Beyer [a,c], Pierluigi Nicotera [a,g], Nasir Ahmad Aziz [a,h], Dan Ehninger [a], Daniele Bano [a,*]

[a] *German Center for Neurodegenerative Diseases (DZNE), Bonn 53127, Germany*
[b] *School of Computer Science, Northwestern Polytechnical University, Xi'an, Shaanxi 710072, China*
[c] *PRECISE Platform for Single Cell Genomics and Epigenomics, DZNE and University of Bonn and West German Genome Center, Bonn 53127, Germany*
[d] *Department of Biomedical Sciences and Padua Center for Network Medicine, University of Padova, Padova 35121, Italy*
[e] *Department of Medical Biometry, Informatics and Epidemiology (IMBIE), Faculty of Medicine, University of Bonn, Bonn 53127, Germany*
[f] *Institute of Innate Immunity, Medical Faculty, University of Bonn, Bonn 53127, Germany*
[g] *IRCCS Mondino Foundation, via Mondino 2, Pavia 27100, Italy*
[h] *University of Bonn, University Hospital Bonn, Institute for Medical Biometry, Informatics and Epidemiology (IMBIE) & Clinic for Parkinson's Disease, Sleep Disorders, and Movement Disorders, Bonn 53127, Germany*

ARTICLE INFO

Keywords:
Aging
Caenorhabditis elegans
Gene transcription
HTZ-1/H2A.Z
Insulin/IGF-1/DAF-2 signaling
Longevity
Metabolism

ABSTRACT

Animal lifespan depends on coordinated gene expression networks that regulate metabolic adaptation, proteostasis, and stress resilience in response to environmental challenges. Histone variants are key regulators of chromatin dynamics, orchestrating nucleosome remodeling, DNA accessibility, and gene expression. While the role of histone H3.3 in aging and animal survival has been explored across model systems, the contribution of other replication-independent histone variants remains less well-defined. Here, we demonstrate that the evolutionarily conserved histone variant HTZ-1/H2A.Z is essential for organismal survival. In the nematode *Caenorhabditis elegans*, loss of HTZ-1/H2A.Z disrupts gene expression programs associated with longevity, including those activated in insulin/IGF-1 deficient *daf-2* mutants and in mitochondrial Complex I deficient animals. Together, our findings show that HTZ-1/H2A.Z regulates gene expression programs that coordinate metabolic and proteostatic pathways, thereby fine-tuning stress responses and promoting lifespan in animals.

1. Introduction

Histones are highly abundant and long-lived proteins (Commerford et al., 1982; Pina and Suau, 1987) that belong to one of the most conserved protein families in the Eukarya domain (Allis and Jenuwein, 2016; Soshnev et al., 2016). In dividing as well as postmitotic cells, histones contribute to the organization of DNA into chromatin, a complex macromolecular structure that packages and regulates access to the genetic information within the nucleus. As the basic building blocks of the chromatin, nucleosomes consist of DNA bound to histone octamers that contain two H2A/H2B dimers and two copies of H3 and H4 (Fierz and Poirier, 2019; Maeshima et al., 2019). To achieve higher-order genomic compaction, the linker histone H1 promotes intra-nucleosome interactions that further inhibit DNA accessibility. All nucleosomal histones have unstructured N- and C-terminal tails that protrude from the globular domains. These flexible tails contain several amino acids that can undergo posttranslational modifications (PTMs) (Millan-Zambrano et al., 2022). These PTMs alter DNA-histone interactions and act as a rich alphabet code to regulate gene transcription, heterochromatin formation, DNA replication and damage response (Allis and Jenuwein, 2016; Millan-Zambrano et al., 2022; Soshnev et al., 2016). As an additional layer of complexity to an extensive combination of epigenetic marks, canonical histones can be replaced by non-canonical histone variants with unique biological properties, including DNA binding and nucleosome stability (Talbert and Henikoff, 2021). These histone variants differ by a few amino acids that are

* Correspondence to: Deutsches Zentrum für Neurodegenerative Erkrankungen (DZNE), Venusberg-Campus 1, Gebäude 99, Bonn 53127, Germany.
E-mail address: daniele.bano@dzne.de (D. Bano).

https://doi.org/10.1016/j.mad.2026.112217
Received 27 November 2025; Received in revised form 11 May 2026; Accepted 22 June 2026
Available online 24 June 2026

essential for their binding to dedicated chaperones (e.g., H3.1 vs H3.3), or they possess longer terminal tails on which distinct PTMs occur (e.g., H2A vs H2A.X). Importantly, the deposition of these histone variants may establish specialized chromatin regions that regulate the recruitment of dedicated molecular machineries involved in various epigenetic programs, such as DNA damage response, gene transcription and silencing (Buschbeck and Hake, 2017; Martire and Banaszynski, 2020; Talbert and Henikoff, 2021). While canonical histones are expressed almost exclusively during the DNA synthesis phase (S phase) by multi-copy genes, replication-independent (RI) histone variants are expressed throughout the cell cycle by one or two intronic genes (Biterge and Schneider, 2014; Martire and Banaszynski, 2020; Talbert and Henikoff, 2021). Apart from histone H4 (only one variant in human cells), all the other histone families have many variants with unique amino acid sequences or domains that account for their distinct biological features (Kurumizaka et al., 2021; Sokolova et al., 2023). For example, RI histone variant H3.3 differs from canonical H3.1 and H3.2 by five and four amino acids, respectively, three of which determine the binding specificity to the dedicated histone H3.3 chaperones (Bano et al., 2017; Buschbeck and Hake, 2017; Sokolova et al., 2023). Among the most studied RI histone variants, the histone H2A.Z is found in all eukaryotes and has unique functional features with profound effects on nucleosome dynamics, regulation of gene transcription and DNA damage response (Diegmuller et al., 2025; Oberdoerffer and Miller, 2023). While H2A.Z shares ~60% of its amino acid sequence with canonical H2A, it has high sequence homology across orthologs in different phyla, suggesting evolutionarily conserved functions in chromatin remodeling (Biterge and Schneider, 2014; Diegmuller et al., 2025; Giaimo et al., 2019). In this regard, H2A.Z-containing nucleosomes are highly enriched at active transcriptional start sites (TSS) and their presence positively correlates with gene expression (Jin and Felsenfeld, 2007; Jin et al., 2009) and euchromatin maintenance (Meneghini et al., 2003). H2A.Z is typically found associated with H3.3 at active promoters and enhancers, with the resulting double variant-containing nucleosomes that are less stable and easily displaceable during transcriptional activation (Giaimo et al., 2019; Henikoff, 2009; Jin and Felsenfeld, 2007; Jin et al., 2009). Consistent with its unique biological roles, genetic deletion of H2Av/H2A.Z causes embryonic lethality in *Drosophila melanogaster* (van Daal and Elgin, 1992). Similarly, RNAi-mediated *htz-1/h2a.z* knockdown affects the temporal development of the pharynx and may cause embryonic lethality of *C. elegans* larvae (Updike and Mango, 2006; Whittle et al., 2008). Although the maternal contribution of HTZ-1 partially restores viability during embryogenesis, *htz-1(null)* alleles cause near-complete sterility in adulthood, with only a few escapers hatching and sometimes reaching the L1 larval stage (Whittle et al., 2008). HTZ-1 is already abundant at the two-cell embryo stage and its incorporation into nucleosomes increases during embryogenesis. In this regard, HTZ-1 is detected at the promoters of the first genes within most of *C. elegans* operons and its presence correlates with the pattern of RNA polymerase II occupancy (Whittle et al., 2008). Finally, H2A.Z knockout does not affect mouse blastocysts development until implantation, although it causes lethality during gastrulation (Faast et al., 2001). Beside embryonic development, H2A.Z also creates essential chromatin states underlying proper differentiation and maintenance of postmitotic cells. For example, H2A.Z knockdown in the pyramidal cell layer of the hippocampus impacts the expression of genes involved in neuronal plasticity and memory performance (Stefanelli et al., 2018; Zovkic et al., 2014). Consistent with its essential role in neural epigenetics, conditional H2A.Z knockout in GABAergic neurons impairs the expression of nuclear-encoded mitochondrial proteins, resulting in aberrant mitochondrial bioenergetics that negatively affect cell survival and causes progressive ataxia in transgenic mice (Lowden et al., 2021). Likewise, muscle-specific H2A.Z loss triggers mitochondrial defects that are associated with increased DNA damage and reduced mouse lifespan (Belotti et al., 2024). All together, these cross-species data indicate that H2A.Z is important for both developmental programs in embryos and epigenetic transcriptional regulation in adult metazoans.

Aging is a progressive biological process and a major risk factor for numerous human disorders, including cancer and neurodegenerative diseases. As a multiscale phenomenon, it is influenced by factors acting across molecular, cellular, tissue and organismal levels (Keshavarz et al., 2023a, 2023b). Among the twelve "hallmarks of aging" (Lopez-Otin et al., 2023), age-associated chromatin defects can alter gene expression patterns that sustain homeostatic processes as well as stress resilience against environmental challenges, with negative consequences for the intracellular maintenance of metabolism and proteome. An abundant literature has shown that inhibition of the insulin/IGF−1/DAF−2 signaling has profound "anti-aging" effects in *C. elegans*, since it promotes health span, pathogen resistance and longevity (Kenyon et al., 1993; Kenyon, 2010; Riera et al., 2016). The remarkable lifespan extension depends on metabolic and stress response programs under the control of transcription factors, such as DAF−16/FOXO (Hsu et al., 2003; Lin et al., 1997, 2001; Ogg et al., 1997). To induce the lifespan extension of *daf−2* mutant nematodes, continuous histone turnover ensures chromatin landscapes that allow the efficient transcriptional regulation of thousands of genes involved in stress resilience and metabolic adaptation to environmental cues, ultimately stimulating longevity (Alvares et al., 2014; Das et al., 2021; Huang et al., 2022; Jin et al., 2011; Piazzesi et al., 2016; Riedel et al., 2013). We and others have demonstrated that the turnover of RI histone variant H3.3 contributes to the establishment of pro-longevity pathways underlying stress resistance in *C. elegans* (Bano et al., 2017; Delaney et al., 2018; Piazzesi et al., 2016, 2022; Strobino et al., 2020). While the role of H3.3 in animal survival has been ascertained, less is known about other RI histone variants and their impact on longevity. Encouraged by our previous works (Bano et al., 2017, 2021; Piazzesi et al., 2016, 2022), we sought to investigate the importance of HTZ-1/H2A.Z in *C. elegans* lifespan. Here, we report that tightly regulated HTZ-1 expression is indispensable for animal survival and the establishment of pro-longevity programs, as shown in Complex I deficient *nuo−6* mutants and IIS deficient *daf−2* mutants. Taking a broader view, HTZ-1 may contribute to the transcriptional regulation of age-related processes.

2. Materials and methods

2.1. Bulk RNA-sequencing and analysis

Synchronized *C. elegans* populations were collected on the first day of young adult and were dissolved in 1 ml Trizol (Invitrogen). For each genotype and mRNA-sequencing analysis, four biological replicates were used. Total RNA was isolated using the RNeasy Micro Kit (Qiagen) according to the manufacturer's protocol. RNA quantity and integrity were evaluated using the High Sensitivity (HS) RNA assay on an Agilent Tapestation 4200 system. For RNA-sequencing, non-strand-specific, full-length transcript libraries were generated following the Smart-seq2 protocol as previously described (Picelli et al., 2014). Briefly, 2 ng of total RNA was added to a reaction buffer containing 0.2% Triton X−100, a protein-based RNase inhibitor, dNTPs, and oligo-dT primers to selectively target polyadenylated mRNA for reverse transcription. The SMART reverse transcription reaction was carried out at 42°C for 90 min using SuperScript II (Invitrogen) in conjunction with a Template-Switching Oligo. The resulting cDNA was subsequently amplified via 16 cycles of pre-amplification PCR to generate double-stranded DNA. Following amplification, 100 pg of cDNA was subjected to tagmentation and enrichment using the Nextera XT Kit (Illumina) to prepare the final sequencing libraries. Library quantification was performed using the Qubit HS dsDNA assay, and fragment size distribution was analyzed using the D1000 assay on an Agilent Tapestation 4200 system. Sequencing was conducted in paired-end mode (2 × 75 bp) on an Illumina NextSeq 2000 System using the NextSeq 2000 P4 XLEAP-SBS™ Reagent Kit (300 Cycles). Demultiplexing of raw

sequencing data was performed using bcl2fastq2 v2.20, and transcript quantification was achieved by aligning reads to the *Caenorhabditis elegans* reference genome (Ensembl release 109) using Kallisto v048.0. The raw RNA-sequencing data for wt, *htz-1(bon101)*, *daf−2(e1370)*, *daf−2(e1370);htz-1(bon101)*, *daf−16(mu86);daf−2(e1370) and daf−16 (mu86);daf−2(e1370);htz-1(bon101)* was deposited in the Gene Expression Omnibus (GEO) database under accession code GSE293787. The raw data used for comparison among *htz-1(bon101)*, *htz-1(tm2469)* and *htz-1(ok3099)* was deposited under accession code GSE328181.

2.2. Caenorhabditis elegans strains and maintenance

Nematodes were maintained on nematode growth media (NGM) in temperature-controlled incubators (20°C). Animals were fed with the B-type (OP50) *Escherichia coli* strain. The following *C. elegans* strains were used: wild type N2 (Bristol), BAN1 *daf−2(e1370)*, BAN155 *daf−16 (mu86);daf−2(e1370)*, BAN502 *htz-1(bon101)/nT1[qIs51]*, BAN734 *nuo−6(qm200);htz-1(bon101)/nT1[qIs51]*, BAN737 *daf−2(e1370);htz-1 (bon101)/nT1[qIs51]*, BAN738 *daf−16(mu86);daf−2(e1370);htz-1 (bon101)/nT1[qIs51]*, MQ1333 *nuo−6(qm200)*, EKM11 *htz-1(tm2469)/ nT1[qIs51]* and VC2480 *htz-1(ok3099)/nT1[qIs51]*. Some strains were provided by the CGC, which is funded by NIH Office of Research Infrastructure Programs (P40 OD010440).

2.3. Database searching

Raw data files were processed with Proteome Discoverer™ software (v3.0.1.27, Thermo Scientific) using SEQUEST® HT search engine against the Swiss-Prot® *Caenorhabditis elegans database* (v2023–11–08). Peptides were identified by specifying trypsin as the protease, with up to 2 missed cleavage sites allowed and restricting peptide length between 7 and 30 amino acids. Precursor mass tolerance was set to 10 ppm, and fragment mass tolerance to 0.02 Da MS2. Static modifications were set as carbamidomethylated cysteine, while dynamic modifications included methionine and N-terminal loss of methionine, for all searches. Peptide and protein FDR were set to 1% by the peptide and protein validator nodes in the Consensus workflow. Default settings of individual nodes were used if not otherwise specified. In the Spectrum Selector node, the Lowest Charge State = 2 and Highest Charge State = 6 were used. The INFERYS rescoring node was set to automatic mode and the resulting peptide hits were filtered for maximum 1% FDR using the Percolator algorithm in the Processing workflow. Both unique and razor peptides were selected for protein quantification. Proteins identified by site, reverse or potential contaminants were filtered out prior to analysis.

2.4. GTEx data preprocessing and linear regression models

The Genotype-Tissue Expression (GTEx) Project was supported by the Common Fund of the Office of the Director of the National Institutes of Health, and by NCI, NHGRI, NHLBI, NIDA, NIMH, and NINDS. The data used for the analyses described in this manuscript were obtained from dbGaP accession number phs000424.v10.p2 NHGRI GTEx on 07/29/2024. We processed bulk RNA-sequencing (RNA-seq) data from 17,350 samples generated by the Genotype-Tissue Expression (GTEx) Project (v8) (Mele et al., 2015), representing 54 human tissue types. Raw sequencing reads were aligned to the GRCh38/hg38 reference genome using STAR aligner, and gene-level quantification was performed using the featureCounts tool (v2.0.8) (Liao et al., 2019; Love et al., 2014), with the following parameters:-g gene_id -t gene -p –countReadPairs -s 0, which specify counting at the gene level (-t gene), using gene IDs from the annotation file (-g gene_id), enabling counting of paired-end reads (-p), counting read pairs instead of individual reads (–countReadPairs), and assuming an unstranded library protocol (-s 0). Gene annotation was based on GENCODE v47, a comprehensive and high-quality reference annotation for human genes. FeatureCounts extracted raw read counts for approximately 86,404 gene variants, encompassing protein-coding genes, long non-coding RNAs, pseudogenes, and other transcript biotypes. To normalize for library size and technical variability, raw counts were processed using the DESeq2 package (v1.42.1) (Love et al., 2014). Size factor normalization was applied, and a variance-stabilizing transformation (VST) was used to stabilize variance across the range of expression values and prepare the data for linear modelling. This preprocessed gene expression matrix served as the basis for our tissue-specific regression analyses of *H2AZ1* and *H2AZ2* gene expression in relation to aging and other covariates. Linear regression was used for analyzing the association of H2AZ1 and H2AZ2 with age. In our model, we regressed gene expression on age, sex, and the top five genotype principal components (PCs): Expression (H2AZ1 or H2AZ2)~Age + Sex + PC1 + … + PC5. This model captures the baseline association of age at tissue procurement with H2AZ1 and H2AZ2 expression while adjusting for genetic population structure and sex. Samples exhibiting high influence in the regression analysis were flagged and excluded based on Cook's distance, a common diagnostic measure for identifying influential outliers in linear models. For determining statistically significant age-associated expression changes, we applied a false discovery rate (FDR) threshold of 0.05, using the Benjamini-Hochberg procedure to correct for multiple testing.

2.5. Lifespan assay

All lifespan assays were carried out at 20°C. Briefly, eggs were isolated from gravid young adults by using an alkaline hypochlorite solution. Then, eggs were transferred on bacteria-seeded NGM plates (day 0 in the lifespan assay) and hatched animals were transferred to fresh agar plates every two days until all animals were dead. For the RNAi experiments, plasmidic RNAi clones (control, *htz-1*, *ama−1 and ife−2* from *E. coli* HT115) (Ahringer library, Geneserivice LDT/Horizon Discovery) were transformed into *E. coli* OP50(xu363) and grown overnight at 37°C in LB media containing ampicillin and tetracycline. A 1:100 dilution of the overnight cultures was then used to grow RNAi clones to OD (600 nm) of 0.2–0.4. Bacteria were plated on NGM plates in the presence of IPTG (1 mM final concentration in the liquid culture) and used the following day for lifespan assays. Dead animals were scored by assessing their response to touch. Nematodes were censored if they died due to internal hatching of eggs or had vulva protrusion. Differences in *C. elegans* survival were determined with the Log-rank (Mantel-Cox) test after survival curves were estimated for each genotype with the Kaplan-Meier method. Statistical significance was determined as $p < 0.05$ and calculated with GraphPad Software Prism 10. Graphs are representative panels of one of the biological replicates reported in Supplementary Table ST1–2 (see also Supplementary Data 5).

2.6. Liquid chromatography tandem mass spectrometry (LC-MS/MS) analysis

Approximately 600–800 young adult nematodes were collected. Total proteins were extracted by lysing the samples in 200 µl Lysis buffer (50 mM HEPES (pH 7.4), 150 mM NaCl, 1 mM EDTA, 1.5% SDS, 1 mM DTT), supplemented with 1x protease and phosphatase inhibitor cocktail (ThermoScientific). The lysis protocol involved repeated cycles of sonication in a water bath (6 cycles of 1 min sonication (35 kHz)), followed by 2 min incubations on ice. At least 20 µg of *C. elegans* protein lysates were reduced and alkylated prior to processing by a modified filter-aided sample preparation (FASP) protocol as previously described (Scifo et al., 2015). On filter Trypsin (1:20; in 50 mM ammonium bicarbonate) digestion of the samples was performed at 37°C, after which the tryptic peptides were precipitated with an equal volume of 2 M KCl to deplete residual detergents. Tryptic peptides were then cleaned, desalted on C18 stage tips and re-suspended in 20 µl 1% FA for LC-MS/MS analysis. MS runs were performed in quadruplicates. Analysis of tryptic peptides was performed using a Dionex Ultimate 3000

RSLC nanosystem coupled to an Orbitrap Exploris 480 MS. Peptides were loaded on a trap column cartridge (Acclaim PepMap C18 100 Å, 5 mm×300 μm i.d., #160454, Thermo Scientific) prior to reversed-phase chromatographic separation on an Acclaim PepMap C18, 100 Å, 75 μm X 50 cm column (ThermoScientific) with starting conditions of 95% eluent A (0.1% FA in water) and 5% eluent B (0.1% FA in 80% ACN). Peptide separation was carried out at 300 nl/min for 120 min using a two-step acetonitrile gradient 8–25% over the first 90 min and 25–50% for the following 30 min. The temperature of the column oven was 55°C. The mass spectrometer was operated in data dependent positive ion mode with MS1 spectra recorded at a resolution of 120 000. Other settings of the MS1 scan included: automatic gain control (AGC) target value of 300% (3×10^6) ions, maximum injection time (maxIT) set to Auto, an intensity threshold of 1×10^4, and mass scan range of 350–1550. Precursor ions for MS/MS were selected using a top speed method with a cycle time of 2 s, an isolation window of 2 *m/z* and normalized collision energy (NCE) of 30% (High-energy Collision Dissociation (HCD)) for fragmentation. MS2 spectra were acquired using a decision tree with a minimum precursor signal intensity threshold of 3×10^5 for scan priority one and an intensity range of 1×10^4 - 3×10^5 for scan priority two. Other MS2 scan settings included: 7.5 K and 15 K resolution (scan priority 1 and 2, respectively), AGC target value of 100% (1×10^5), maxIT set to 20 and 50 ms, for scan priority one and two, respectively. Full MS data were acquired in the profile mode with fragment spectra recorded in the centroid mode. Raw MS data is publicly available under the following accession numbers-ProteomeXchange (PXD063184) and jPOST (JPST003765) via the following link: https://repository.jpostdb.org/entry/ JPST003765.

2.7. Puromycin assay and western blotting

Synchronized *C. elegans* adults were collected and washed three times with S-basal. Then, animals were incubated in puromycin-containing S-basal (composed of 20μl of heat-inactivated OP50 bacteria, 170 μl of S-basal, 10 μl of 10 mg/ml puromycin (Sigma, P9620), resulting in a final puromycin concentration of 0.5 mg/ml) at 20°C in a thermomixer with constant shaking at 300 rpm. Untreated animals (as negative controls) were incubated under the same conditions but without puromycin. After 4 h, animals were pelleted and stored at −80℃. Samples were sonicated in ice-cold RIPA buffer (Sigma) supplemented with protease and phosphatase inhibitors. Whole lysates were centrifuged at 2000*g* for 5 min at 4℃, and the supernatant were collected for protein quantification using Bradford reagent (Sigma). Proteins were denatured by boiling in Laemmli buffer at 95℃ for 5 min. Approximately 20 μg of total proteins were loaded into each well of 15% polyacrylamide gels and separated by SDS-PAGE. Proteins were then transferred onto nitrocellulose membranes (Bio-Rad) using Trans-Blot Turbo semi-dry transfer system (Bio-Rad). Membranes were blocked with 5% BSA in 0.05% TBST and incubated overnight at 4℃ with an anti-puromycin antibody. Blots were washed in 0.05% TBST for 30 min, followed by incubation with secondary antibodies for 1 h at room temperature. After a 30-minute wash, blots were imaged using LI-COR Odyssey Infrared Imaging System. Subsequently, membranes were incubated with an anti-α-tubulin antibody for 2 h at room temperature. After washing, secondary antibody incubation and imaging were performed as described above, using a lower exposure for the anti-α-tubulin signal. Band intensities were quantified using ImageJ. The intensities of the entire lanes of puromycin-labelling were normalized to that of tubulin. The following antibodies were used: mouse monoclonal anti-puromycin (3RH11, Kerafast, EQ0001, 1:500), mouse monoclonal anti-α-tubulin (clone B−5–1–2, Sigma-Aldrich, T6074, 1:5000), IRDye 680RD Goat anti-Mouse IgG (LI-COR Biosciences, 926–68070, 1:10000). To assess HTZ-1 protein levels, wt (N2) and *htz-1* mutant animals were collected and washed three times in water. Then, animals were pelleted and flash-frozen in liquid nitrogen. Samples were lysed in RIPA buffer (with protease and phosphatase inhibitors), sonicated for two cycles of 15 s each, and centrifuged at 1200*g* for 15 min at 4°C. Supernatants were collected and protein concentration was determined using a Bradford assay. Laemmli loading buffer was added to denature proteins at 95°C for 5 min. Equal amounts of proteins were separated by SDS-PAGE and transferred onto a nitrocellulose membrane. Membranes were blocked in 5% milk in 0.05% TBS-T for 1 h and incubated overnight at 4°C with the primary antibody (histone H2A.Z polyclonal antibody ThermoFisher, PA5–116156; dilution 1:1000). The following day, membranes were washed three times with 0.05% TBS-T for 10 min each, followed by incubation with the secondary antibodies, goat anti-rabbit HRP (dilution 1:2000). Membranes were washed three times again and incubated with mouse monoclonal anti-α-tubulin (clone B−5–1–2, Sigma-Aldrich, T6074; dilution 1:5000) antibodies for 2 h. HRP-conjugated secondary antibodies were used to develop blots by incubating membranes with enhanced chemiluminescence (ECL) substrate (Pierce, ThermoFisher Scientific). A Bio-Rad Chemidoc system was used to detect signals. ImageJ was used for densitometry.

2.8. Statistics

Transcript abundances were quantified using Kallisto and imported into R (v4.5.3) using the tximport package (v1.38.2). Gene level counts were scaled using the lengthScaledTPM method. Sample metadata were constructed based on experimental groups, where strain was defined as the design variable. Genes with low expression (less than 10 counts in at least two samples) were prefiltered prior to analysis. Normalization, dispersion estimation and model fitting were performed using the default DESeq2 workflow. Analyses of differentially expressed genes were performed in R usingDESeq2 package (v1.50.2), and the results for the comparisons were obtained using the Wald test. Log2 fold change shrinkage was applied using the apeglm method (v1.32.0). Volcano plots were generated to visualize differential expression results. Genes were classified as significantly upregulated or downregulated based on thresholds of $|\log2 \text{ fold change shrunk}| > 1$ and $\text{padj} < 0.05$. Adjusted p-values of zero were replaced with the smallest positive value to enable log transformation for visualization purposes. Gene Set Enrichment Analysis (GSEA) was carried out using a ranked list of genes ordered by their Wald statistic obtained from DESeq2. For proteomics, significant proteins were selected if $|\log2 \text{ fold change}| > 0.585$ and $\text{padj} < 0.05$. GraphPad Prism Software was used to calculate statistics. The Mann-Whitney test (non-parametric) was used to compare two groups, whereas ANOVA (with appropriate post hoc corrections) was employed for three or more groups. Statistical significance was defined as $p < 0.05$. The number of biological replicates is indicated in the figures. For lifespan assays, Kaplan-Meier survival curves and the Log-rank (Mantel-Cox) test was used to estimate statistical significance.

3. Results

3.1. H2A.Z expression is associated with organismal aging and regulates animal lifespan

To define the relationship between chronological aging and the expression of *H2AZ1* and *H2AZ2* genes, we performed tissue-wise linear regression across 54 human tissues based on RNA-seq data from the 17350 Genotype-Tissue Expression (GTEx) samples. Both *H2AZ1* and *H2AZ2* genes showed a negative association with chronological aging, across multiple tissues. Specifically, *H2AZ1* was significantly downregulated in 17 tissues (FDR < 0.05), including brain-amygdala, brain-caudate (basal ganglia) and skeletal muscle, while it was upregulated in one tissue (artery aorta) (Fig. 1A and Supplementary Data 1). Similarly, *H2AZ2* expression exhibited a significant age-associated downregulation in 18 tissues (e.g., brain-caudate, brain-cerebellar hemisphere, brain-nucleus accumbens, heart-atrial appendage, heart-left ventricle) (Fig. 1A and Supplementary Data 1). Furthermore, we found that in breast tissue *H2AZ1/H2AZ2* expression was significantly lower in

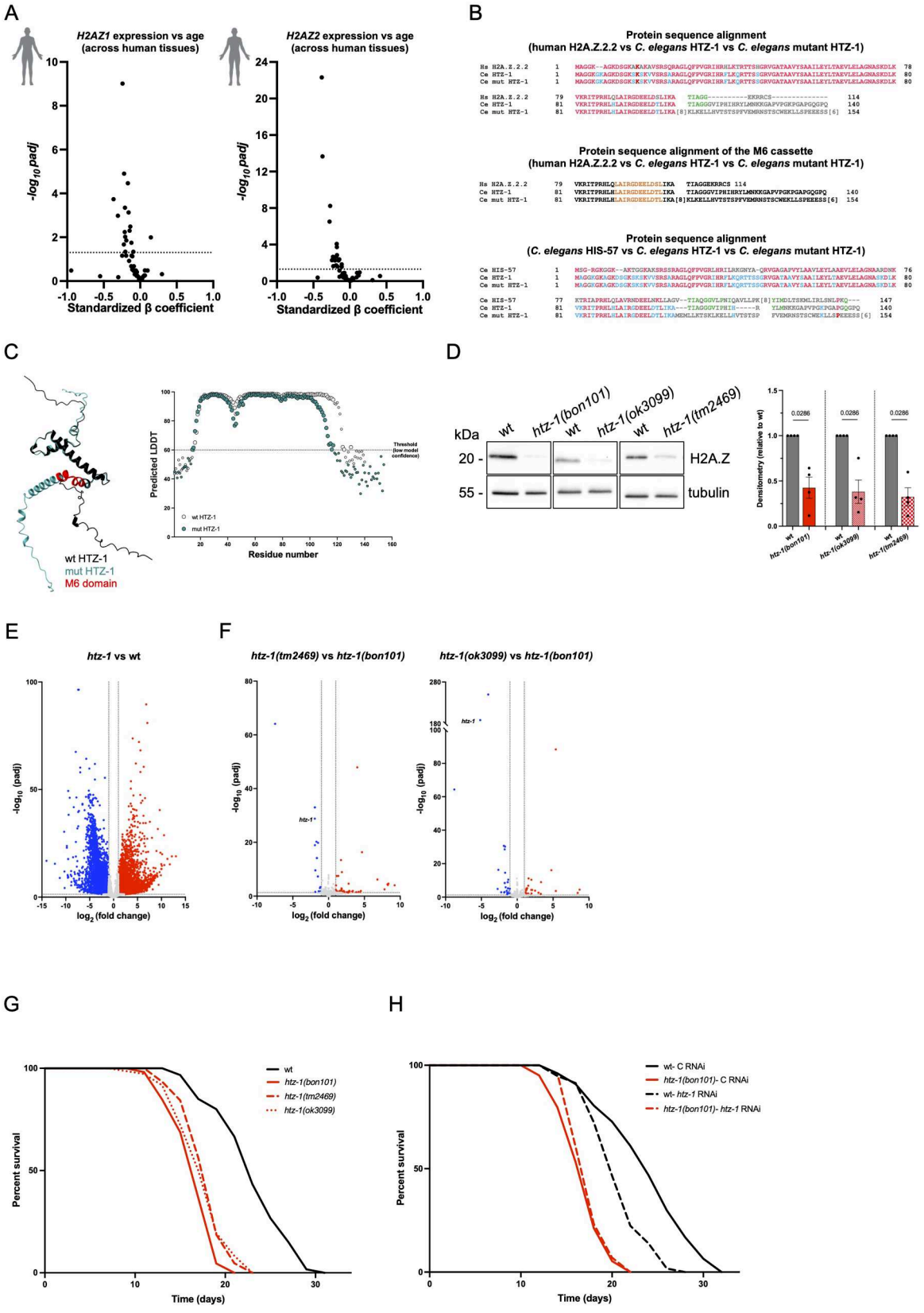

(caption on next page)

Fig. 1. HTZ-1/H2A.Z is required for *C. elegans* survival. (A) Volcano plots depict the -log$_{10}$(adj-p value) on the y-axis against the estimated regression coefficient (β) for age on the x-axis, showing results from Model 1. The gene expression (variance-stabilized counts) was regressed on age, sex, and the first five genotype principal components. Each point represents a single tissue's association of *H2AZ1* (left panel) or *H2AZ2* (right panel) expression with age. Positive β values (right) indicate age-associated upregulation; negative β values (left) indicate downregulation. Horizontal dashed lines correspond to a false discovery rate (FDR) threshold of 0.05. (B) Alignments of protein sequences obtained by using constraint-based multiple alignment tool (COBALT). Top and middle panels report protein sequence alignments of human (Hs) H2A.Z.2.2, *C. elegans* (Ce) HTZ-1 and mutant (mut) HTZ-1. Bottom panel is the alignment of *C. elegans* HIS−57, HTZ-1 and mutant (mut) HTZ-1. Color coding is as follows: red indicates amino acids conserved across the three variants; cyan and green indicate homologous sequences between two variants; orange highlights the M6 domain (as annotated in Uniprot). (C) AlphaFold predicted structures of wild type (black) and mutant (dark cyan) HTZ-1, with the M6 domain highlighted in red. The predicted local distance difference test (pLDDT) is reported in the panel on the right. Threshold (dot line) indicates low model confidence (<60). (D) Representative immunoblots of samples from wt (N2), *htz-1(bon101), htz-1(ok3099)* and *htz-1(tm2469)* animals using an antibody against HTZ-1/H2A.Z (tubulin as loading control). Densitometry is reported on the right (n = 4, mean±SEM, Mann-Whitney test; *p* values are reported). (E-F) Volcano plot of differentially expressed genes in *htz-1(bon101)* mutants compared to (E) wt, (F) *htz-1(tm2469)* and *htz-1(ok3099)* mutant animals. (G) Representative lifespan assays of *htz-1* mutants compared to wt. Genotypes of the *htz-1* mutant strains are indicated. (H) Lifespan assay of wt (N2) and *htz-1(bon101)* mutant animals on control (C) and *htz-1* RNAi (OP50 bacteria).

females, whereas in pituitary tissue it was significantly higher compared to males (Supplementary Data 2). Across other tissues, there were no apparent robust sex differences. Together, these data demonstrate that both *H2AZ1* and *H2AZ2* are downregulated across multiple tissues in humans during aging, suggesting a role for H2A.Z in age-associated gene expression patterns.

To better understand the role of HTZ-1 in age-related processes and survival, we employed CRISPR/Cas9 gene editing and manipulated the endogenous *htz-1* locus. Rather than generating large deletions that could potentially affect the expression of neighboring genes, we sought to obtain an HTZ-1/H2A.Z variant still having the C-terminal acidic residues (the M6 region, Fig. 1B) that are critical for its deposition (Clarkson et al., 1999; Jensen et al., 2011; Ridgway et al., 2004; Subramanian et al., 2013). After an initial screening of positive hits, we identified an allele that encoded a predicted protein with high homology with the human H2A.Z.2.2 isoform (Fig. 1B). Based on DNA sequencing, the frameshift mutation was downstream of the evolutionarily conserved M6 region and resulted in a C-terminal region that did not share significant homology with either wild type HTZ-1 or H2A variant HIS−57 (Fig. 1B-C). Western blot analysis revealed that HTZ-1 protein levels were comparable between our newly generated mutants and two previously reported strains expressing *htz-1(null)* alleles (Petty et al., 2009) (Fig. 1D and Supplementary Figure S1A). Bulk RNA-sequencing revealed almost 6000 differentially expressed genes in *htz-1(bon101)* mutants compared with young adult wt nematodes (Fig. 1E and Supplementary Data 3). In contrast, the global transcriptional profile of *htz-1(bon101)* was highly similar to those of *htz-1(tm2469)* and *htz-1(ok3099)* mutants, both of which carry deletions that disrupt *htz-1* mRNA expression (Fig. 1F and Supplementary Data 3). As for other *htz-1 loss of function (lof)* alleles, *htz-1(bon101)* caused sterility of homozygous adult hermaphrodites and therefore it was maintained with the *nT1* balancer, a relatively stable translocation of portions of Chromosome IV and V. Lifespan assays showed that *htz-1(bon101)* animals lived approximately 9 days less than wild type (wt) *C. elegans*, while the median lifespan was comparable to *htz-1(tm2469)* and *htz-1(ok3099)* mutants (Fig. 1G and Supplementary Table ST1). Double-stranded RNA against *htz-1* significantly reduced wt (N2) survival, whereas it had no additive effect on *htz-1(bon101)* lifespan (Fig. 1H and Supplementary Table ST2). At least under the growth conditions employed here, these data suggest that *htz-1(bon101)* is a *(lof)* allele that affects animal survival.

3.2. HTZ-1 loss affects processes associated with epigenetics and metabolism

To better understand the transcriptional alterations associated with the reduced lifespan of *htz-1(bon101)* mutants, we performed Gene Set Enrichment Analysis (GSEA) om a genome-wide ranked transcriptomic dataset to identify significantly enriched Gene Ontology (GO) categories, including biological processes, molecular functions and cellular components. As expected, HTZ-1 loss led to an enrichment of GO terms related to chromatin organization, RNA polymerase II activity and DNA binding, reflecting HTZ-1/H2A.Z's role in epigenetics (Fig. 2A). Complementary KEGG pathway analyses highlighted significant enrichment in genes involved in carbon metabolism and mitochondrial bioenergetics (Fig. 2B-C and Supplementary Figure S1B), suggesting that HTZ-1 influences coordinated expression programs underlying nuclear and metabolic functions. To corroborate our RNA-sequencing data, we performed a proteomic analysis and found ~600 proteins that were differentially expressed in *htz-1(bon101)* mutants compared to wt *C. elegans* (Fig. 2D and Supplementary Data 4). The expression of several mitochondrial, metabolic and stress response proteins showed partial correlation with their corresponding transcriptional profiles (Fig. 2E-F and Supplementary Figure S1C-F). Given the KEGG enrichment for processes associated with mitochondrial bioenergetics and carbon metabolism, we hypothesized that HTZ-1 loss could impact the longevity pathways that depend on mitochondria. As in some of our previous studies (Gioran et al., 2014, 2019; Jackson et al., 2022; Piazzesi et al., 2016, 2022), we employed Complex I deficient *nuo−6(qm200)* mutant nematodes, which live longer than wt animals as a consequence of transcriptional modulation of several pro-longevity pathways. Consistent with the important role of chromatin remodeling in survival of mitochondrial mutant nematodes (Merkwirth et al., 2016; Piazzesi et al., 2016; Tian et al., 2016), loss of HTZ-1/H2A.Z variant negatively affected the lifespan-extending properties of Complex I dysfunction, with *nuo−6(qm200);htz-1(bon101)* mutants having a lifespan comparable to wt nematodes (Fig. 2G and Supplementary Table ST1). These data suggest that HTZ-1 is required to translate mitochondria-derived signals into transcriptional profiles inducing longevity.

3.3. Inhibition of protein synthesis and RNA polymerase II fails to rescue the lifespan reduction of htz-1 mutants

We performed additional GSEA GO enrichment analyses, which revealed significant alterations in chromatin maintenance and remodeling, as well as protein synthesis (Fig. 3A-C). Notably, several transcriptional changes were not reflected at the proteomic level (Supplementary Figure S1C-F), as exemplified by canonical histones, whose protein expression showed no correlation with RNA-sequencing data (Fig. 3D-E). These observations suggested that HTZ-1 loss might broadly affect the global rate of protein synthesis. To test this, we conducted a puromycin incorporation assay in adult animals. Immunoblot analyses revealed a clear trend toward reduced puromycin incorporation into newly synthesized proteins in *htz-1(bon101)* mutants (Fig. 3F), which may explain the observed discrepancy between transcriptional and proteomic profiles (Supplementary Figure S1C-F). To determine whether inhibition of protein synthesis or RNA polymerase II activity could influence *htz-1* lifespan, we exposed wt and *htz-1(bon101)* mutant animals to *ife−2* (Syntichaki et al., 2007) or *ama−1* RNAi, respectively. While both RNAi treatments significantly affected the lifespan of wt animals, they had no effect on *htz-1(bon101)* survival (Fig. 3G and Supplementary Table ST2), indicating that the shortened lifespan caused

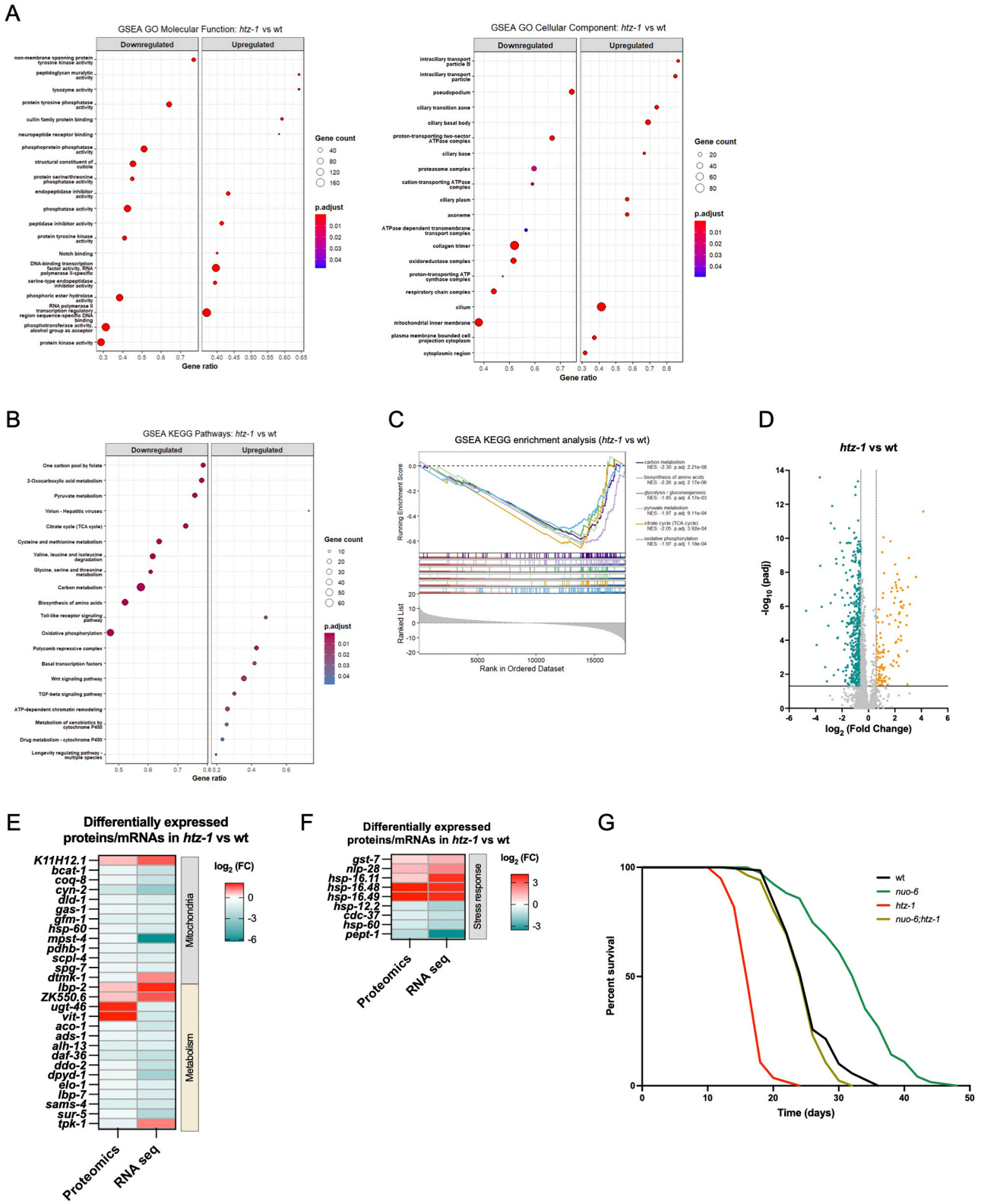

Fig. 2. HTZ-1 alters metabolism and mitochondria-dependent longevity signals. (A-C) Gene Set Enrichment Analysis (GSEA) performed based on the ranked list of all detected genes in *htz-1(bon101)* vs wt. (A) Top 20 enriched Gene Ontology (GO) in the molecular function and cellular component categories. (B) Top 20 enriched KEGG pathways identified in *htz-1(bon101)* vs wt. (C) Significant downregulation of key metabolic gene sets identified from GSEA-based KEGG analysis in *htz-1(bon101)* vs wt. (D) Volcano plot for the proteomic analysis of *htz-1(bon101)* vs wt animals. Up- and down-regulated proteins are in orange and green, respectively. (E-F) Heat maps of genes and proteins that are significantly altered in *htz-1(bon101)* mutants compared to wt animals. Mitochondrial and metabolic proteins are reported in (E), while stress response factors are in (F). (G) Representative lifespan assay of wt, *nuo−6(qm200)*, *htz-1(bon101)* and *nuo−6(qm200);htz-1 (bon101)* mutants.

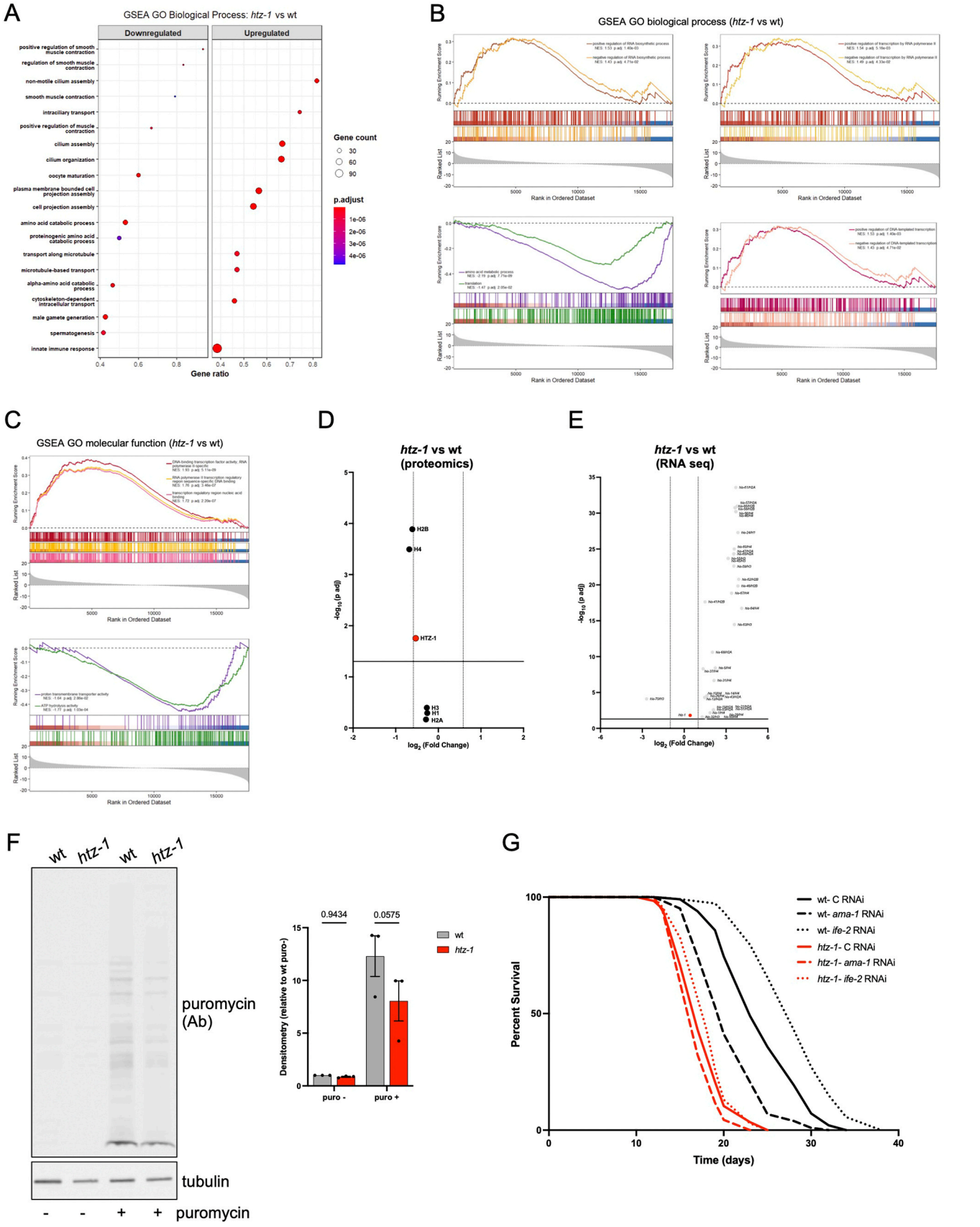

(caption on next page)

Fig. 3. HTZ-1 loss is associated with aberrant protein synthesis. (A-B) GSEA GO biological process analysis performed based on the ranked list of all detected genes in *htz-1(bon101)* vs wt. (A) Top 20 enriched GO biological process terms. (B) Enrichment curves for gene sets derived from GSEA GO biological process analyzed using RNA-seq data of *htz-1(bon101)* vs wt animals. The similarity of the enrichment curves in the top-left and bottom-right panels reflects the overlap in leading-edge gene between the corresponding GO terms. (C) Enrichment curves for translation- and transcription- related gene sets derived from GSEA GO molecular function category in *htz-1(bon101)* vs wt. (D-E) Volcano plots of (D) proteomic and (E) RNA-sequencing data relative to histones. HTZ-1 protein and *htz-1* mRNA are highlighted as red dots. (F) Puromycin assay in wt and *htz-1(bon101)* nematodes. After 4 h, untreated (-) and puromycin-treated (+) animals were collected and immunoblots performed by using an antibody against newly synthesized puromycin-containing proteins. Densitometric quantification is shown on the right. Puromycin signal intensities were normalized to α-tubulin (as a loading control) and presented relative to wt puro-(first lane) (n = 3, two-way ANOVA; *p* values are reported). (G) Representative lifespan assay of wt and *htz-1(bon101)* mutant nematodes grown on control, *ama−1* and *ife−2* RNAi bacteria.

by HTZ-1 loss cannot be rescued by reducing protein synthesis or inhibiting RNA polymerase II activity.

3.4. HTZ-1 deficiency negatively affects daf−2 longevity

Next, we investigated whether the *htz-1(bon101)* allele could affect the lifespan-extending properties of the hypomorphic *daf−2(e1370)* mutation, a well-characterized allele that inhibits insulin/IGF−1 signaling in *C. elegans* (Kenyon et al., 1993; Kimura et al., 1997) (Fig. 4A). RNA-sequencing analysis revealed that 2465 genes were significantly upregulated and 2202 genes were downregulated in *daf−2;htz*-1 double mutants compared with *daf−2* single mutants (Fig. 4B and Supplementary Data 3). Unbiased GSEA confirmed that many dysregulated genes in *daf−2;htz*-1 mutants were associated with metabolism, such as carbon metabolism and amino acid metabolism, as well as with longevity regulating pathways (Fig. 4C-D). Complementary proteomic analyses revealed more than 600 proteins that were differentially regulated in *daf−2;htz*-1 mutants compared to *daf−2* animals (Fig. 4E and Supplementary Data 4). Similar to *htz-1* vs wt comparison (Supplementary Figure S1C-F), we observed discordant trends between mRNA and protein levels in *daf−2;htz*-1 mutants compared to *daf−2* animals (Supplementary Figure S2A-D). Notably, 21 histone-related transcripts and their encoded variants exhibited opposite changes in *daf−2;htz*-1 mutants compared to *daf−2* animals (Fig. 4F and Supplementary Figure 2D), whereas several differentially expressed mitochondrial proteins, metabolic enzymes and stress response-related proteins displayed concordant trends at both mRNA and protein levels (Fig. 4G and Supplementary Figure S2C). These transcriptional and proteomic changes prompted us to examine whether HTZ-1 loss could also affect the longevity of IIS mutants. To do so, we performed lifespan assays and, similar to H3.3 deficiency (Piazzesi et al., 2016, 2022), HTZ-1 loss shortened the lifespan of *daf−2(e1370)* mutants by approximately 21 days (Fig. 4H and Supplementary Table ST1). In summary, our data suggest that HTZ-1 is required to sustain gene expression in IIS mutants.

3.5. HTZ-1 loss shortens the survival of daf−16;daf−2 mutant C. elegans

Since DAF−2 signaling depends on DAF−16/FOXO (Kimura et al., 1997; Lin et al., 1997; Ogg et al., 1997) (Fig. 4A), we generated *daf−16 (mu86);daf−2(e1370);htz-1(bon101)* triple mutants and compared their transcriptional and proteomic profiles with *daf−16;daf−2* double mutant animals (Fig. 5A-D, Supplementary Figure S3A-B and Supplementary Data 3–4). RNA-sequencing analysis identified 3148 genes significantly upregulated and 2677 genes downregulated in *daf−16; daf−2;htz-1* mutants compared to *daf−16;daf−2* (Fig. 5C). GSEA of these differentially expressed genes revealed a pronounced enrichment of pathways related to ribosome components, mitochondrial function and chromatin organization (Fig. 5E-F), highlighting the broad impact of HTZ-1 loss on regulatory networks underlying gene expression programs that govern protein synthesis, cellular bioenergetics and chromatin architecture in the context of IIS. Notably, HTZ-1 loss further impacted the transcriptional profiles in *daf−16;daf−2* mutants (Fig. 5C-D and Supplementary Figure S3C), suggesting an additive effect. Consistent with our observations in other mutant backgrounds, the majority of transcriptional changes in *daf−16;daf−2;htz-1* triple mutants were not mirrored by corresponding alterations at the protein level, indicating a widespread discordance between mRNA abundance and protein expression (Supplementary Figure S3D-G). To complete our survey, we performed lifespan assays and found that *daf−16;daf−2;htz-1* lived approximately 8 days less compared to *daf−16(mu86);daf−2(e1370)* mutants (Fig. 5G and Supplementary Table ST1), consistent with our hypothesis of an additive effect in IIS deficient animals lacking DAF−16. In summary, these findings indicate that HTZ-1 expression is required to elicit transcriptional programs and corresponding proteomes supporting lifespan-extending signals (Fig. 5H).

4. Discussion

The establishment of longevity pathways is a dynamic process that requires the transcriptional regulation of thousands of genes supporting proteostasis, metabolic adaptation and stress resilience (Bar-Ziv et al., 2020; Denzel et al., 2019; Mannick and Lamming, 2023; Rodriguez-Colman et al., 2024). Across species, histone PTMs and histone variant turnover serve as crucial epigenetic marks that regulate the precise recruitment of chromatin remodelers, which may exert either activating or repressive effects on gene expression. Failure to regulate these pro-longevity gene expression profiles can negatively affect cells' ability to respond to environmental challenges, with severe consequences on animal survival, development of chronic diseases and aging trajectories. Building on our prior work on RI histone variant H3.3 (Piazzesi et al., 2016, 2022), we undertook an investigation on HTZ-1/H2A.Z, since it is an essential histone variant that is highly conserved across species. We employed the nematode *C. elegans*, which expresses canonical histone H2A and HTZ-1/H2A.Z, but it does not express any known macroH2A and *bona fide* H2A.X, the latter having a few complementary, though still distinct functions with H2A.Z (e.g., DNA damage repair) (Diegmuller et al., 2025; Giaimo et al., 2019; Oberdoerffer and Miller, 2023; Talbert and Henikoff, 2021). We generated a *htz-1(lof)* allele that resulted in phenotypes similar to existing *htz-1(lof)* alleles (Petty et al., 2009; Whittle et al., 2008), including sterility in adult hermaphrodites. Here, we report the critical involvement of histone variant HTZ-1/H2A.Z in regulating longevity pathways and aging-related processes. Contrary to H3.3 deficiency (Piazzesi et al., 2016, 2022), loss of HTZ-1 variant significantly altered transcriptional profiles in wt and long-lived mutant nematodes, with detrimental consequences on *C. elegans* survival. Based on our RNA-sequencing and proteomic data, we observed changes in the expression of genes involved in mitochondria, metabolism and stress response, further highlighting the importance of histone HTZ-1/H2A.Z in mitochondrial homeostasis as previously shown in transgenic mice (Lowden et al., 2021). Of note, *htz-1(bon101)* animals displayed higher expression levels of many genes encoding canonical core histones, which were not paralleled by a proteomic signature with a similar trend. Based on our *in vivo* puromycin assay, we found that *htz-1* mutants showed a reduced global protein synthesis compared to wt animals, possibly explaining some of the differences that we observed at the transcriptional and proteomic levels. As our analyses were performed in whole organisms, we cannot rule out that these changes occurred in the germline cells in an attempt to compensate for defective HTZ-1/H2A.Z dynamics. Alternatively, defects in HTZ-1/H2A.Z dynamics may cause genomic instability and consequent expression of genes that are tightly repressed in

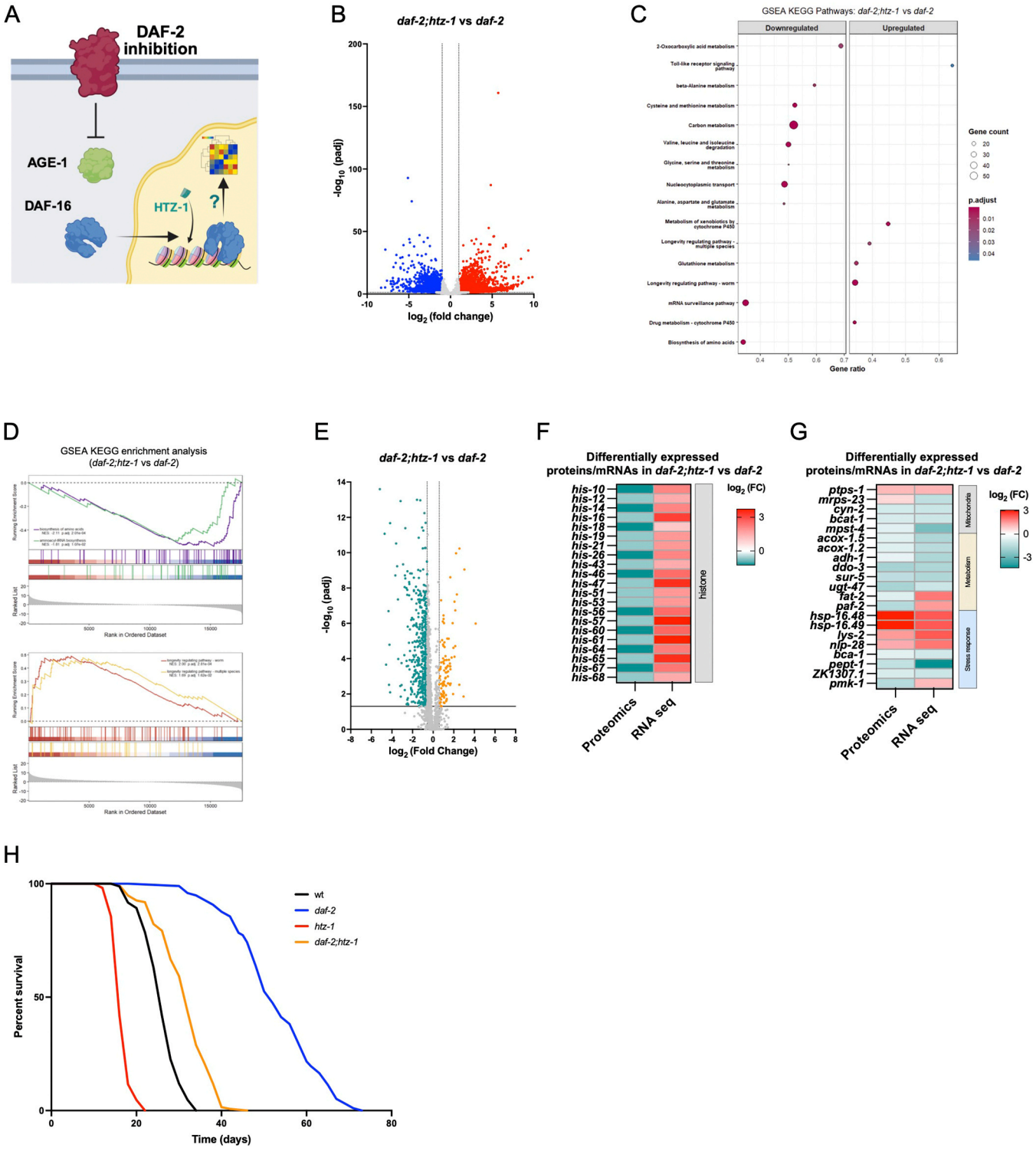

Fig. 4. HTZ-1 expression sustains the lifespan extension of *daf−2* mutants. (A) Schematic representation of the insulin/IGF−1/DAF−2 signaling pathway. In *daf−2* mutants, AGE−1/PI3K does not phosphorylate DAF−16, which can translocate to the nucleus to induce gene transcription. The contribution of HTZ-1 to DAF−2-dependent transcriptional programs remains elusive. (B) Volcano plots of up- and down-regulated genes in *daf−2(e1370);htz-1(bon101)* compared to *daf−2 (e1370)* animals. (C) Top 20 enriched GSEA KEGG pathways based on RNA-seq data of *daf−2(e1370);htz-1(bon101)* vs *daf−2(e1370)*. (D) Enrichment curves of amino acids biosynthesis and longevity gene sets based on GSEA KEGG results in *daf−2(e1370);htz-1(bon101)* compared to *daf−2(e1370)* animals. (E) Volcano plot of up- and down-regulated proteins in *daf−2(e1370);htz-1(bon101)* compared to *daf−2(e1370)* animals. (F-G) Heat maps of (F) histones and (G) mitochondrial, metabolic, stress response factors that are dysregulated in both proteomics and RNA-sequencing datasets in *daf−2(e1370);htz-1(bon101)* compared to *daf−2(e1370) C. elegans*. (H) Representative lifespan assay of wt, *htz-1(bon101)*, *daf−2(e1370)* and *daf−2(e1370);htz-1(bon101)* animals.

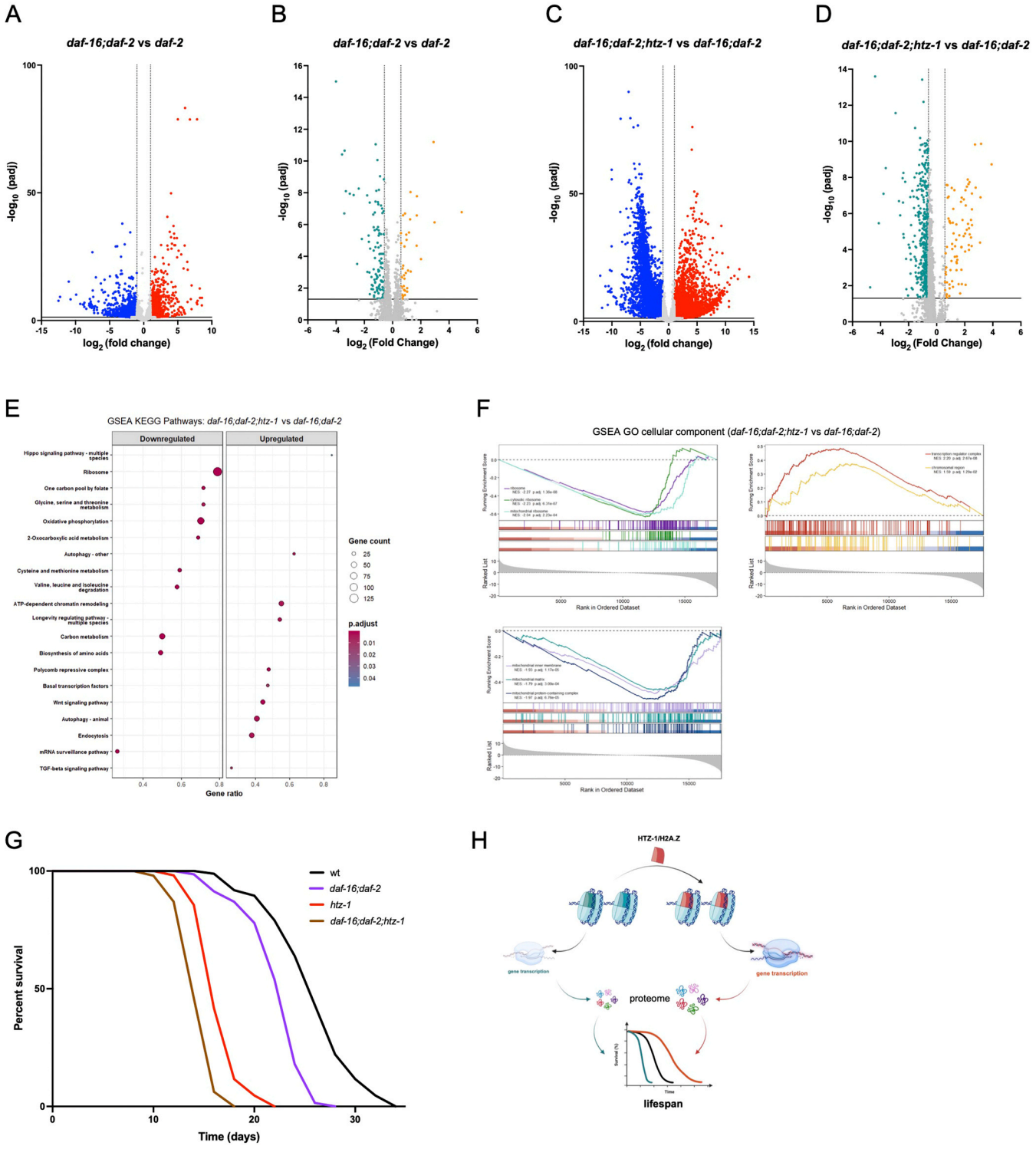

Fig. 5. HTZ-1 loss shortens the lifespan of *daf−16;daf−2* mutants. (A-B) Volcano plots of (A) RNA-sequencing and (B) proteomic data of *daf−16(mu86);daf−2 (e1370)* vs *daf−2(e1370)* mutants. (C-D) Volcano plots of (C) RNA-sequencing and (D) proteomic data in *daf−16(mu86);daf−2(e1370);htz-1(bon101)* vs *daf−16 (mu86);daf−2(e1370)* mutants. (E) Top 20 enriched GSEA KEGG pathways based on RNA-seq data of *daf−16(mu86);daf−2(e1370);htz-1(bon101)* vs *daf−16(mu86); daf−2(e1370)* animals. (F) Enrichment curves of ribosome-, mitochondria- and chromatin/transcription-related gene sets for GSEA GO cellular component analysis in *daf−16(mu86);daf−2(e1370);htz-1(bon101)* vs *daf−16(mu86);daf−2(e1370)* animals. (G) Representative survival assay of wt, *daf−16(mu86);daf−2(e1370)*, *htz-1 (bon101)*, *daf−16(mu86);daf−2(e1370);htz-1(bon101)* mutant animals. (H) Schematic summary of our findings. HTZ-1/H2A.Z regulates gene expression underlying longevity. Loss of HTZ-1/H2A.Z compromises the maintenance of transcriptional proteomic profiles that are required to sustain animal survival.

somatic cells. While H3.3 deficiency had a minor impact on survival and gene transcription compared to wt, HTZ-1/H2A.Z loss had profound long-term consequences on animal health. Strikingly, we demonstrate that HTZ-1 has a strong impact on DAF−2 signaling. The effects on pro-longevity transcriptional processes go beyond DAF−16-dependent targets, as shown by our comparative analyses in *daf−2*, *daf−16;daf−2* and *nuo−6* mutant backgrounds. Since *C. elegans* does not express all H2A variants described in mammals, it may be that in lower organisms HTZ-1/H2A.Z is involved in additional biological processes (e.g., DNA double-strand break repair) that are usually controlled by other histone H2A variants. Alternatively, HTZ-1/H2A.Z may be deposited onto genomic regions encoding highly transcribed genes that are essential for promoting longevity pathways.

5. Limitations and conclusions

We recognize the limitations of our study, as our findings have not been validated in other model systems. Furthermore, we are aware that future investigations will be essential to elucidate the molecular mechanisms underlying HTZ-1 dynamics, including deposition and turnover, in pro-longevity processes. At the same time, our results provide an initial snapshot into the role of HTZ-1/H2A.Z in gene expression programs that regulate lifespan and age-related processes, which further underscore the relevance of epigenetics as one of the key "hallmarks" of aging (Keshavarz et al., 2023b; Lopez-Otin et al., 2023).

CRediT authorship contribution statement

Matthias Schmid: Supervision. **Diego De Stefani:** Supervision. **Mrityunjoy Mondal:** Formal analysis, Investigation. **Stefan Paulusch:** Investigation, Formal analysis. **Rossella Erminia Ciliberti:** Formal analysis, Investigation. **Elena De Domenico:** Investigation, Formal analysis. **Ioanna-Maria Menegatou:** Formal analysis, Investigation, Visualization. **Jialu Hu:** Visualization, Investigation, Formal analysis. **Daniele Bano:** Writing – original draft, Visualization, Supervision, Project administration, Funding acquisition, Formal analysis, Conceptualization. **Antonia Piazzesi:** Investigation. **Dan Ehninger:** Resources. **Yiru Wang:** Investigation. **Nasir Ahmad Aziz:** Supervision, Resources. **Enzo Scifo:** Visualization, Investigation, Formal analysis. **Pierluigi Nicotera:** Funding acquisition. **Beijia Xie:** Visualization, Investigation, Formal analysis. **Beyer Marc:** Resources. **Dagmar Wachten:** Supervision.

Funding

This research was supported by the DZNE institutional budget. BX was supported by a China Scholarship Council (CSC) fellowship (grant number 202108110050). IMM is supported by the Deutsche Forschungsgemeinschaft (DFG, German Research Foundation)- SPP2453, project number 541647076 (DB: grant recipient). This work was supported by the Ministry of Culture and Science of North Rhine-Westphalia. NGS analyses were carried out at the Joint Scientific Facility WGGC-Bonn PRECISE.

Declaration of generative AI and AI-assisted technologies in the manuscript preparation process

During the preparation of this work, text-generating AI tools (ChatGPT, Google Gemini) helped to improve language and readability of a few sentences. After using these tools, the corresponding author reviewed and edited the content and takes full responsibility for the content of the published article.

Declaration of Competing Interest

The authors declare no financial or non-financial competing interests.

Acknowledgements

We wish to express our gratitude to Ms. Christiane Bartling-Kirsch and Michael Kraut for their technical support. We would like to thank colleagues at InVivo Biosystems (Eugene, Oregon, USA) for their help with *C. elegans* gene editing. DB, MDB and DW are members of the Excellence Cluster ImmunoSensation^2 (Deutsche Forschungsgemeinschaft DFG- EXC2151- 390873048). DB and DE are members of the ETERNITY project consortium (EU Horizon Europe MSCA-DN, grant number 101072759). DB is member of the consortium "EPIADAPT" funded by Deutsche Forschungsgemeinschaft (DFG, German Research Foundation: 563430056/SPP2502). Some of the schemes were created in BioRender.com (Bano, D. (2026) https://BioRender.com/59zaa27).

Appendix A. Supporting information

Supplementary data associated with this article can be found in the online version at doi:10.1016/j.mad.2026.112217.

Data availability

All data have been deposited in publicly accessible repositories.

References

Allis, C.D., Jenuwein, T., 2016. The molecular hallmarks of epigenetic control. Nat. Rev. Genet. 17, 487–500.
Alvares, S.M., Mayberry, G.A., Joyner, E.Y., Lakowski, B., Ahmed, S., 2014. H3K4 demethylase activities repress proliferative and postmitotic aging. Aging Cell. 13, 245–253.
Bano, D., Piazzesi, A., Salomoni, P., Nicotera, P., 2017. The histone variant H3.3 claims its place in the crowded scene of epigenetics. Aging 9, 602–614.
Bano, D., Salomoni, P., Ehninger, D., Nicotera, P., 2021. The histone code in dementia: Transcriptional and chromatin plasticity fades away. Curr. Opin. Pharmacol. 60, 117–122.
Bar-Ziv, R., Bolas, T., Dillin, A., 2020. Systemic effects of mitochondrial stress. EMBO Rep. 21, e50094.
Belotti, E., Lacoste, N., Iftikhar, A., Simonet, T., Papin, C., Osseni, A., Streichenberger, N., Mari, P.O., Girard, E., Graies, M., Giglia-Mari, G., Dimitrov, S., Hamiche, A., Schaeffer, L., 2024. H2A.Z is involved in premature aging and DSB repair initiation in muscle fibers. Nucleic Acids Res. 52, 3031–3049.
Biterge, B., Schneider, R., 2014. Histone variants: key players of chromatin. Cell. Tissue Res. 356, 457–466.
Buschbeck, M., Hake, S.B., 2017. Variants of core histones and their roles in cell fate decisions, development and cancer. Nat. Rev. Mol. Cell. Biol. 18, 299–314.
Clarkson, M.J., Wells, J.R., Gibson, F., Saint, R., Tremethick, D.J., 1999. Regions of variant histone His2AvD required for Drosophila development. Nature 399, 694–697.
Commerford, S.L., Carsten, A.L., Cronkite, E.P., 1982. Histone turnover within nonproliferating cells. Proc. Natl. Acad. Sci. USA 79, 1163–1165.
Das, S., Min, S., Prahlad, V., 2021. Gene bookmarking by the heat shock transcription factor programs the insulin-like signaling pathway. Mol. Cell. 81, 4843–4860 e4848.
Delaney, K., Mailler, J., Wenda, J.M., Gabus, C., Steiner, F.A., 2018. Differential expression of histone H3.3 genes and their role in modulating temperature stress response in Caenorhabditis elegans. Genetics 209, 551–565.
Denzel, M.S., Lapierre, L.R., Mack, H.I.D., 2019. Emerging topics in C. elegans aging research: Transcriptional regulation, stress response and epigenetics. Mech. Ageing Dev. 177, 4–21.
Diegmuller, F., Leers, J., Hake, S.B., 2025. The "Ins and Outs and What-Abouts" of H2A.Z: A tribute to C. David Allis. J. Biol. Chem. 301, 108154.
Faast, R., Thonglairoam, V., Schulz, T.C., Beall, J., Wells, J.R., Taylor, H., Matthaei, K., Rathjen, P.D., Tremethick, D.J., Lyons, I., 2001. Histone variant H2A.Z is required for early mammalian development. Curr. Biol. 11, 1183–1187.
Fierz, B., Poirier, M.G., 2019. Biophysics of chromatin dynamics. Annu. Rev. Biophys. 48, 321–345.
Giaimo, B.D., Ferrante, F., Herchenrother, A., Hake, S.B., Borggrefe, T., 2019. The histone variant H2A.Z in gene regulation. Epigenetics Chromatin 12, 37.
Gioran, A., Nicotera, P., Bano, D., 2014. Impaired mitochondrial respiration promotes dendritic branching via the AMPK signaling pathway. Cell. Death Dis. 5, e1175.
Gioran, A., Piazzesi, A., Bertan, F., Schroer, J., Wischhof, L., Nicotera, P., Bano, D., 2019. Multi-omics identify xanthine as a pro-survival metabolite for nematodes with mitochondrial dysfunction. EMBO J. 38.
Henikoff, S., 2009. Labile H3.3+H2A.Z nucleosomes mark 'nucleosome-free regions. Nat. Genet. 41, 865–866.

Hsu, A.L., Murphy, C.T., Kenyon, C., 2003. Regulation of aging and age-related disease by DAF-16 and heat-shock factor. Science 300, 1142–1145.
Huang, M., Hong, M., Hou, X., Zhu, C., Chen, D., Chen, X., Guang, S., Feng, X., 2022. H3K9me1/2 methylation limits the lifespan of daf-2 mutants in C. elegans. Elife 11.
Jackson, J., Wischhof, L., Scifo, E., Pellizzer, A., Wang, Y., Piazzesi, A., Gentile, D., Siddig, S., Stork, M., Hopkins, C.E., Handler, K., Weis, J., Roos, A., Schultze, J.L., Nicotera, P., Ehninger, D., Bano, D., 2022. SGPL1 stimulates VPS39 recruitment to the mitochondria in MICU1 deficient cells. Mol. Metab., 101503
Jensen, K., Santisteban, M.S., Urekar, C., Smith, M.M., 2011. Histone H2A.Z acid patch residues required for deposition and function. Mol. Genet. Genom. 285, 287–296.
Jin, C., Felsenfeld, G., 2007. Nucleosome stability mediated by histone variants H3.3 and H2A.Z. Genes. Dev. 21, 1519–1529.
Jin, C., Zang, C., Wei, G., Cui, K., Peng, W., Zhao, K., Felsenfeld, G., 2009. H3.3/H2A.Z double variant-containing nucleosomes mark 'nucleosome-free regions' of active promoters and other regulatory regions. Nat. Genet. 41, 941–945.
Jin, C., Li, J., Green, C.D., Yu, X., Tang, X., Han, D., Xian, B., Wang, D., Huang, X., Cao, X., Yan, Z., Hou, L., Liu, J., Shukeir, N., Khaitovich, P., Chen, C.D., Zhang, H., Jenuwein, T., Han, J.D., 2011. Histone demethylase UTX-1 regulates C. elegans life span by targeting the insulin/IGF-1 signaling pathway. Cell. Metab. 14, 161–172.
Kenyon, C., Chang, J., Gensch, E., Rudner, A., Tabtiang, R., 1993. A C. elegans mutant that lives twice as long as wild type. Nature 366, 461–464.
Kenyon, C.J., 2010. The genetics of ageing. Nature 464, 504–512.
Keshavarz, M., Xie, K., Bano, D., Ehninger, D., 2023a. Aging - What it is and how to measure it. Mech. Ageing Dev. 213, 111837.
Keshavarz, M., Xie, K., Schaaf, K., Bano, D., Ehninger, D., 2023b. Targeting the "hallmarks of aging" to slow aging and treat age-related disease: fact or fiction? Mol. Psychiatry 28, 242–255.
Kimura, K.D., Tissenbaum, H.A., Liu, Y., Ruvkun, G., 1997. daf-2, an insulin receptor-like gene that regulates longevity and diapause in Caenorhabditis elegans. Science 277, 942–946.
Kurumizaka, H., Kujirai, T., Takizawa, Y., 2021. Contributions of histone variants in nucleosome structure and function. J. Mol. Biol. 433, 166678.
Liao, Y., Smyth, G.K., Shi, W., 2019. The R package Rsubread is easier, faster, cheaper and better for alignment and quantification of RNA sequencing reads. Nucleic Acids Res. 47, e47.
Lin, K., Dorman, J.B., Rodan, A., Kenyon, C., 1997. daf-16: An HNF-3/forkhead family member that can function to double the life-span of Caenorhabditis elegans. Science 278, 1319–1322.
Lin, K., Hsin, H., Libina, N., Kenyon, C., 2001. Regulation of the Caenorhabditis elegans longevity protein DAF-16 by insulin/IGF-1 and germline signaling. Nat. Genet. 28, 139–145.
Lopez-Otin, C., Blasco, M.A., Partridge, L., Serrano, M., Kroemer, G., 2023. Hallmarks of aging: An expanding universe. Cell 186, 243–278.
Love, M.I., Huber, W., Anders, S., 2014. Moderated estimation of fold change and dispersion for RNA-seq data with DESeq2. Genome Biol. 15, 550.
Lowden, C., Boulet, A., Boehler, N.A., Seecharran, S., Rios Garcia, J., Lowe, N.J., Liu, J., Ong, J.L.K., Wang, W., Ma, L., Cheng, A.H., Senatore, A., Monks, D.A., Liu, B.H., Leary, S.C., Cheng, H.M., 2021. Homeostatic control of nuclear-encoded mitochondrial gene expression by the histone variant H2A.Z is essential for neuronal survival. Cell. Rep. 36, 109704.
Maeshima, K., Ide, S., Babokhov, M., 2019. Dynamic chromatin organization without the 30-nm fiber. Curr. Opin. Cell. Biol. 58, 95–104.
Mannick, J.B., Lamming, D.W., 2023. Targeting the biology of aging with mTOR inhibitors. Nat. Aging 3, 642–660.
Martire, S., Banaszynski, L.A., 2020. The roles of histone variants in fine-tuning chromatin organization and function. Nat. Rev. Mol. Cell. Biol. 21, 522–541.
Mele, M., Ferreira, P.G., Reverter, F., DeLuca, D.S., Monlong, J., Sammeth, M., Young, T. R., Goldmann, J.M., Pervouchine, D.D., Sullivan, T.J., Johnson, R., Segre, A.V., Djebali, S., Niarchou, A., Consortium, G.T., Wright, F.A., Lappalainen, T., Calvo, M., Getz, G., Dermitzakis, E.T., Ardlie, K.G., Guigo, R., 2015. Human genomics. The human transcriptome across tissues and individuals. Science 348, 660–665.
Meneghini, M.D., Wu, M., Madhani, H.D., 2003. Conserved histone variant H2A.Z protects euchromatin from the ectopic spread of silent heterochromatin. Cell 112, 725–736.
Merkwirth, C., Jovaisaite, V., Durieux, J., Matilainen, O., Jordan, S.D., Quiros, P.M., Steffen, K.K., Williams, E.G., Mouchiroud, L., Tronnes, S.U., Murillo, V., Wolff, S.C., Shaw, R.J., Auwerx, J., Dillin, A., 2016. Two conserved histone demethylases regulate mitochondrial stress-induced longevity. Cell 165, 1209–1223.
Millan-Zambrano, G., Burton, A., Bannister, A.J., Schneider, R., 2022. Histone post-translational modifications - cause and consequence of genome function. Nat. Rev. Genet. 23, 563–580.
Oberdoerffer, P., Miller, K.M., 2023. Histone H2A variants: diversifying chromatin to ensure genome integrity. Semin. Cell. Dev. Biol. 135, 59–72.
Ogg, S., Paradis, S., Gottlieb, S., Patterson, G.I., Lee, L., Tissenbaum, H.A., Ruvkun, G., 1997. The Fork head transcription factor DAF-16 transduces insulin-like metabolic and longevity signals in C. elegans. Nature 389, 994–999.
Petty, E.L., Collette, K.S., Cohen, A.J., Snyder, M.J., Csankovszki, G., 2009. Restricting dosage compensation complex binding to the X chromosomes by H2A.Z/HTZ-1. PLoS. Genet. 5, e1000699.
Piazzesi, A., Papic, D., Bertan, F., Salomoni, P., Nicotera, P., Bano, D., 2016. Replication-Independent Histone Variant H3.3 controls animal lifespan through the regulation of pro-longevity transcriptional programs. Cell. Rep. 17, 987–996.
Piazzesi, A., Wang, Y., Jackson, J., Wischhof, L., Zeisler-Diehl, V., Scifo, E., Oganezova, I., Hoffmann, T., Gomez Martin, P., Bertan, F., Wrobel, C.J.J., Schroeder, F.C., Ehninger, D., Handler, K., Schultze, J.L., Schreiber, L., van Echten-Deckert, G., Nicotera, P., Bano, D., 2022. CEST-2.2 overexpression alters lipid metabolism and extends longevity of mitochondrial mutants. EMBO Rep. 23, e52606.
Picelli, S., Faridani, O.R., Bjorklund, A.K., Winberg, G., Sagasser, S., Sandberg, R., 2014. Full-length RNA-seq from single cells using Smart-seq2. Nat. Protoc. 9, 171–181.
Pina, B., Suau, P., 1987. Changes in histones H2A and H3 variant composition in differentiating and mature rat brain cortical neurons. Dev. Biol. 123, 51–58.
Ridgway, P., Brown, K.D., Rangasamy, D., Svensson, U., Tremethick, D.J., 2004. Unique residues on the H2A.Z containing nucleosome surface are important for Xenopus laevis development. J. Biol. Chem. 279, 43815–43820.
Riedel, C.G., Dowen, R.H., Lourenco, G.F., Kirienko, N.V., Heimbucher, T., West, J.A., Bowman, S.K., Kingston, R.E., Dillin, A., Asara, J.M., Ruvkun, G., 2013. DAF-16 employs the chromatin remodeller SWI/SNF to promote stress resistance and longevity. Nat. Cell. Biol. 15, 491–501.
Riera, C.E., Merkwirth, C., De Magalhaes Filho, C.D., Dillin, A., 2016. Signaling networks determining life span. Annu. Rev. Biochem. 85, 35–64.
Rodriguez-Colman, M.J., Dansen, T.B., Burgering, B.M.T., 2024. FOXO transcription factors as mediators of stress adaptation. Nat. Rev. Mol. Cell. Biol. 25, 46–64.
Scifo, E., Szwajda, A., Soliymani, R., Pezzini, F., Bianchi, M., Dapkunas, A., Debski, J., Uusi-Rauva, K., Dadlez, M., Gingras, A.C., Tyynela, J., Simonati, A., Jalanko, A., Baumann, M.H., Lalowski, M., 2015. Proteomic analysis of the palmitoyl protein thioesterase 1 interactome in SH-SY5Y human neuroblastoma cells. J. Proteom. 123, 42–53.
Sokolova, V., Sarkar, S., Tan, D., 2023. Histone variants and chromatin structure, update of advances. Comput. Struct. Biotechnol. J. 21, 299–311.
Soshnev, A.A., Josefowicz, S.Z., Allis, C.D., 2016. Greater than the sum of parts: complexity of the dynamic epigenome. Mol. Cell. 62, 681–694.
Stefanelli, G., Azam, A.B., Walters, B.J., Brimble, M.A., Gettens, C.P., Bouchard-Cannon, P., Cheng, H.M., Davidoff, A.M., Narkaj, K., Day, J.J., Kennedy, A.J., Zovkic, I.B., 2018. Learning and Age-Related changes in genome-wide H2A.Z binding in the mouse Hippocampus. Cell. Rep. 22, 1124–1131.
Strobino, M., Wenda, J.M., Padayachy, L., Steiner, F.A., 2020. Loss of histone H3.3 results in DNA replication defects and altered origin dynamics in C. elegans. Genome Res. 30, 1740–1751.
Subramanian, V., Mazumder, A., Surface, L.E., Butty, V.L., Fields, P.A., Alwan, A., Torrey, L., Thai, K.K., Levine, S.S., Bathe, M., Boyer, L.A., 2013. H2A.Z acidic patch couples chromatin dynamics to regulation of gene expression programs during ESC differentiation. PLoS. Genet. 9, e1003725.
Syntichaki, P., Troulinaki, K., Tavernarakis, N., 2007. eIF4E function in somatic cells modulates ageing in Caenorhabditis elegans. Nature 445, 922–926.
Talbert, P.B., Henikoff, S., 2021. Histone variants at a glance. J. Cell. Sci. 134.
Tian, Y., Garcia, G., Bian, Q., Steffen, K.K., Joe, L., Wolff, S., Meyer, B.J., Dillin, A., 2016. Mitochondrial stress induces chromatin reorganization to promote longevity and UPR(mt). Cell 165, 1197–1208.
Updike, D.L., Mango, S.E., 2006. Temporal regulation of foregut development by HTZ-1/H2A.Z and PHA-4/FoxA. PLoS. Genet. 2, e161.
van Daal, A., Elgin, S.C., 1992. A histone variant, H2AvD, is essential in Drosophila melanogaster. Mol. Biol. Cell. 3, 593–602.
Whittle, C.M., McClinic, K.N., Ercan, S., Zhang, X., Green, R.D., Kelly, W.G., Lieb, J.D., 2008. The genomic distribution and function of histone variant HTZ-1 during C. elegans embryogenesis. PLoS. Genet. 4, e1000187.
Zovkic, I.B., Paulukaitis, B.S., Day, J.J., Etikala, D.M., Sweatt, J.D., 2014. Histone H2A.Z subunit exchange controls consolidation of recent and remote memory. Nature 515, 582–586.